Longitudinal Drifts of Streamers across the Heliospheric Current Sheet

Morgan, Huw

Published in:
Astrophysical Journal

DOI:
10.1088/0004-637X/738/2/190

Publication date:
2011

Citation for published version (APA):
Morgan, H. (2011). Longitudinal Drifts of Streamers across the Heliospheric Current Sheet. *Astrophysical Journal*, *738*(2), 190. https://doi.org/10.1088/0004-637X/738/2/190

The Astrophysical Journal, 738:190 (6pp), 2011 September 10 doi:10.1088/0004-637X/738/2/190

LONGITUDINAL DRIFTS OF STREAMERS ACROSS THE HELIOSPHERIC CURRENT SHEET

Huw Morgan
Institute for Astronomy, University of Hawaii, 2680 Woodlawn Drive, Honolulu, HI 96822, USA; hmorgan@ifa.hawaii.edu
Received 2011 June 2; accepted 2011 July 6; published 2011 August 25

ABSTRACT

Potential field source surface (PFSS) extrapolations of the photospheric magnetic field provide a qualitatively correct model of the coronal magnetic structure. We show that the magnetic structure provided by PFSS describes a framework within which high-density coronal streamers are distributed. However, the density structures have considerable freedom to drift longitudinally along the magnetic structure. Some caution must therefore be taken when using PFSS models as proxies for the coronal density structure. In particular, while measurements of coronal rotation using PFSS models provide an estimate of the large-scale magnetic structure rotation, they are not valid measurements of the density rotation. Furthermore, attempts to assign a consistent rate of rotation to the electron corona over long time periods are not always valid since the movement is dominated by structural reconfiguration. These conclusions are reached by the application of solar rotational tomography to LASCO C2/*Solar and Heliospheric Observatory* observations during solar minimum (1996–1997), revealing the changing density structure of the equatorial streamer belt at a height of 4 $R_{\odot}$.

Key words: solar wind – Sun: corona – Sun: heliosphere – Sun: magnetic topology – Sun: rotation

1. INTRODUCTION

The magnetic structure revealed by potential field source surface (PFSS) models (Altschuler & Newkirk 1969; Schatten et al. 1969; Wang & Sheeley 1992) is widely used as a proxy for density structure in the solar corona and, using further appropriate extrapolation, in the heliosphere. The correct interpretation of PFSS model results does give a topologically correct distribution of magnetic structure (Wang et al. 2007; Morgan & Habbal 2010b). In contrast to the standard interpretation, this interpretation allows the existence of high-density streamers in regions not necessarily associated with a polarity inversion (or the neutral line of the heliospheric current sheet). Both Saez et al. (2005) and Morgan & Habbal (2007) show that streamers lie in regions not associated with a polarity inversion, and Wang et al. (2007) and Morgan & Habbal (2010b) prove unambiguously that high-density streamers are associated with thin sheet-shaped regions where magnetic field lines have emerged from widely separated latitudes at the Sun—whether there is a polarity reversal or not. Morgan & Habbal (2010b) call this value "convergence." Regions of the extended radial corona which contain magnetic field lines originating from widely separated regions at the photosphere are regions of high convergence, and high-density streamers are constrained to exist at these regions. Despite the basic correctness of PFSS models, one of their shortcomings is the lack of consideration of plasma, and of plasma heating mechanisms and time evolution, within the model. It is purely an extrapolation of the observed large-scale photospheric field into a radial extended corona at the source surface. While the magnetic structure provides valuable constraints on where high-density streamers will be found, it does not predict how the density is distributed within that structure. Fortunately, an analysis technique called solar rotational tomography (SRT) can give a tight observational constraint on the coronal density structure. In many ways, SRT provides an excellent complement to PFSS models since one provides an observation of density structure and the other provides a reasonably correct estimate of the magnetic structure.

Studying the structure of the extended solar corona is difficult since a coronagraph image reveals only the line-of-sight (LOS) integration of the optically thin coronal emission. SRT is a method to reveal the three-dimensional (3D) structure of the corona by using a series of observations made over a period of half a solar rotation. Frazin (2000) gives a good summary of the topic. There are now many works which use SRT to study the coronal structure (Kramar et al. 2009; Vásquez et al. 2010, for example). Morgan et al. (2009) introduced a new SRT approach based on Fourier backprojection of height-normalized coronagraph images (Morgan et al. 2006). A more comprehensive overview of the topic of coronal density structure and SRT is given by Morgan & Habbal (2010b). SRT studies of the evolution of coronal structure over time are rare. A comprehensive overview of the changing coronal structure revealed by tomography over a solar activity cycle is given by Morgan & Habbal (2010b), with selected case studies of certain Carrington rotations. The use of SRT to estimate coronal rotation over long timescales is described by Morgan (2011).

This paper describes and discusses an important aspect of the solar minimum corona structural evolution found during the rotational study of Morgan (2011). The method is briefly summarized in Section 2, with references to fuller descriptions of the tomography and time analysis. A set of tomography maps for solar minimum is compared to a corresponding set of PFSS maps in Section 3. Section 4 summarizes the conclusions.

2. METHOD

The most common observation mode for the LASCO C2 coronagraph (Brueckner et al. 1995) is to make a total brightness observation approximately every 20 minutes. Observations made over half a solar rotation are needed to create one tomography map, and, assuming uninterrupted observations, this is a data set containing typically a thousand images. Coronal mass ejections (CMEs) are rapid events which disrupt the tomographical process, and a CME separation technique based on ideas described by Morgan & Habbal (2010a) is used to lessen their influence. Further data processing steps, and the main Fourier backprojection tomographical technique, are described in full by Morgan et al. (2009) and in Morgan (2011).

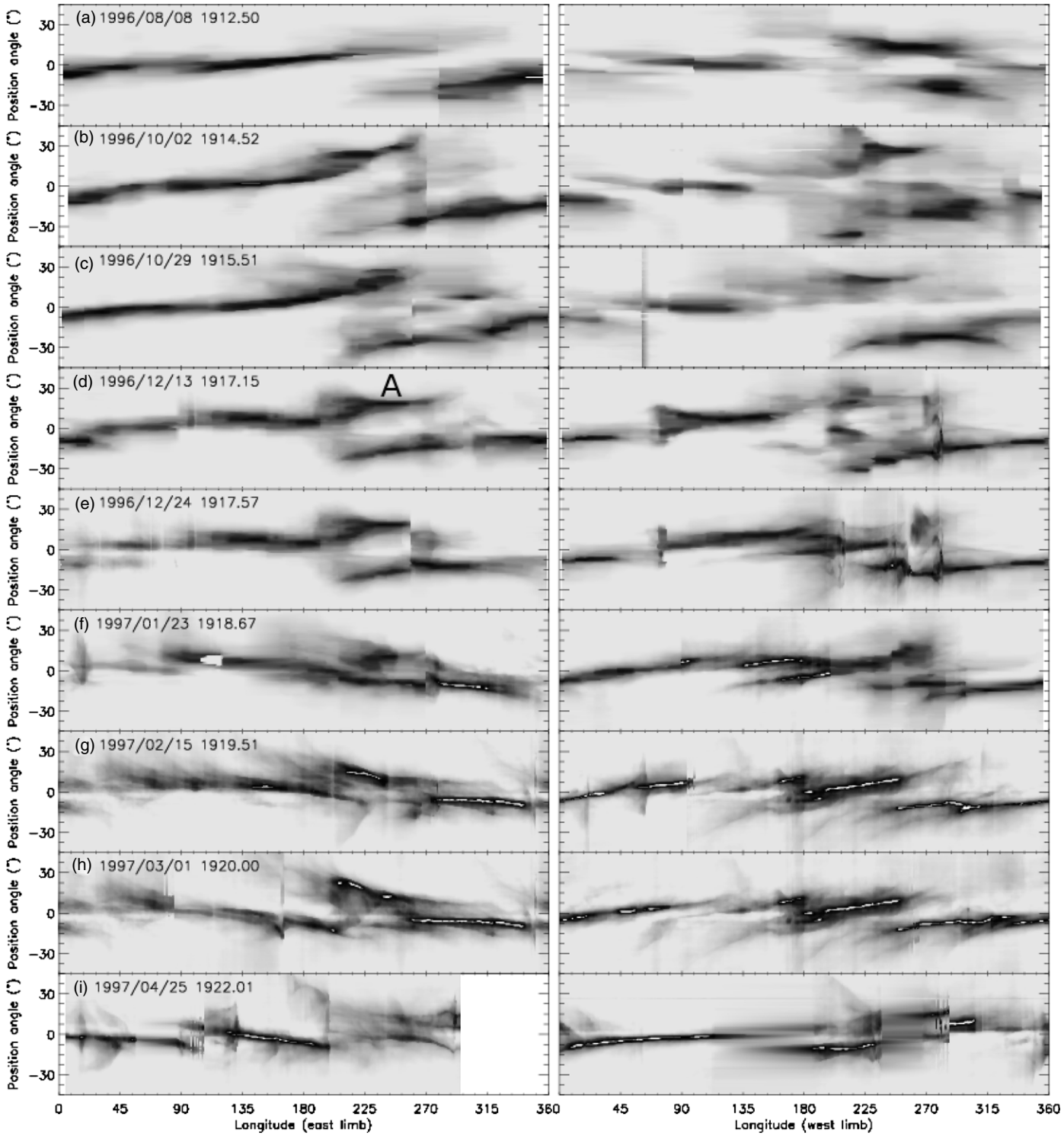

Figure 1. Synoptic maps of LASCO C2 observed brightness at a height of 4 $R_\odot$ for the east limb (left column) and west limb (right column). The brightness scale is inverted (black/white is high/low brightness). For each observation, a slice of a few pixels width surrounding a heliocentric height of 4 $R_\odot$ is taken from the coronagraph images and separated to the east and west limbs. For the time of observation, the Carrington longitude at the east and west limbs is calculated. The east and west limb brightness profiles are then stacked vertically according to Carrington longitude in these plots. Only the position angle range of $-45°$to $45°$ from each equator is shown. To create the $360°$ longitude coverage, around 27 days of observations are needed. This time period is centered on the date shown for each map. The structure labeled A is discussed in the text.

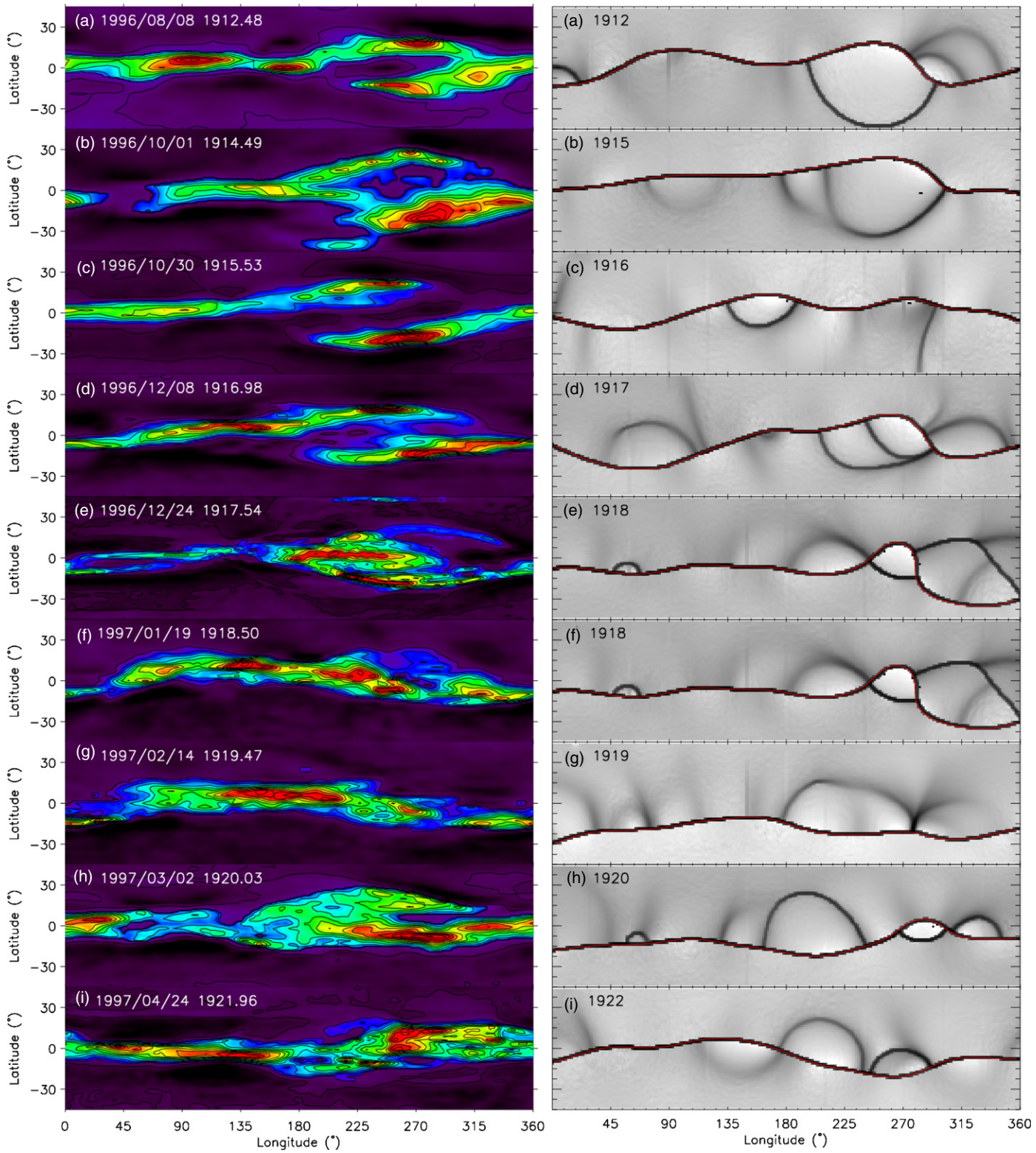

Figure 2. Left column: nine density maps for different observing periods during solar minimum (in time order from top to bottom). The displayed latitude of each map is limited to −45° to 45°. The apparent increase in finer structural detail, or complexity, from the first map (CR 1912.5) to the last (CR 1922.0) is due to the increasing frequency of suitable observations made by LASCO C2, which enables a finer spatial resolution. Red is the highest density, blue/black is low density. Right column: convergence maps (logarithmic scale) calculated from a PFSS extrapolation of photospheric magnetic field measurement made by the Wilcox Solar Observatory (WSO; see acknowledgments) at times as close as possible to the observation periods of the LASCO tomographic maps shown in the left column. Lightly shaded areas show low convergence (field lines have arisen from approximately the same region on the photosphere), and dark regions have high convergence (field lines have arisen from widely separated regions on the photosphere). The red curves show the region where field lines of opposite sign meet (i.e., the heliospheric current sheet). This always coincides with high-convergence values.

The tomography reconstructions made for this work are shells of the corona at a height of 4 $R_\odot$, with 720 longitude bins and 360 latitude bins. When a specific date or Carrington rotation is assigned to a density map, it refers to the mid-time of the half-solar-rotation period used to create the density map. Rotation rate units are given throughout in sidereal degree per day, deg d^{-1}, and are often given relative to the sidereal Carrington rotation rate of 14.18 deg d^{-1} (or a sidereal rotation period of 25.38 d). Conversions from synodic to sidereal are made using the formulation of Roša et al. (1995).

3. RESULTS AND DISCUSSION

Figure 1 highlights the problem of analyzing structure directly from LOS integrated brightness images. The panels show synoptic maps of observed brightness at a height of 4 $R_\odot$ for both east and west limbs. As high-density structures at latitudes other than the equator rotate in and out of the field of view, they form curves which start at higher position angle than their true latitude, then drop in position angle toward the equator until their true latitude is reached. The same process happens in reverse as they rotate out of the plane of sky. One such structure is labeled "A" in panel (d) of Figure 1. Another problem is that longitudinally aligned density structures (forming a long path along the LOS) appear very bright, while structures of the same density, aligned with a north–south orientation (or any angle not along the LOS), appear less bright and may easily be interpreted as a lower density structure, or may be missed completely due to their faintness. For these, and other reasons, the most effective study of coronal structure, or of rotation, is made by first estimating the 3D density structure using tomography.

The left column of Figure 2 shows several density maps resulting from the tomography reconstruction during solar minimum (CR 1912–1922, or 1996 August–1997 May). They contain the main structural aspects of the equatorial streamer belt, namely a high-density equatorial streamer belt composed of longitudinally extended sheets. At some longitudes, two or three sheets can share the same longitude (i.e., the streamer belt diverges into several distinct branches). There is a large variation in the density structure along the streamer belt. The most prominent feature of the equatorial streamer belt at this time is the splitting of the belt into two branches between longitudes 200°and 330°. This two-branch feature has been discussed in detail elsewhere—Saez et al. (2005) is a dedicated study, and it is also discussed in Morgan & Habbal (2010b), and references therein. From CR 1912.5 to 1918.5 (a six-month period), the northern branch of the split is associated with the neutral sheet (the position of which is determined by a PFSS model, shown in the right column of Figure 2). The southern branch is a "pseudostreamer," or convergence sheet not associated with a magnetically neutral region. The sequence of maps shown in the left column of Figure 2 shows the split in the streamer belt persisting from CR1912.5 (1996 August 8) to CR1917.5 (1996 December 23). There seems to be a three-branch split by CR1917.5—which is a sign that a large-scale reconfiguration is occurring. Between CR1918.5 and CR1919.4 (1997 January 19–February 15) the two-branch configuration has disappeared in the density maps although the bend in the PFSS model estimate of the magnetic neutral line remains. By CR1920.0 (1997 March 2) the two-branch configuration reappears.

The right column of Figure 2 shows magnetic convergence within a PFSS model extrapolation. Using the results of a PFSS model, open field lines at the coronal source surface (2.5 $R_\odot$) are traced back to their photospheric origin. The angular distance from each field line's photospheric source to the source of its neighboring field lines is calculated, and the convergence (or the average angular distance) is then assigned to each point on the source surface. Therefore, the convergence maps show a high convergence at the equatorial streamer belt since the field lines there have converged from widely separated regions on the Sun (they arise from mid-latitudes at the north and south and are forced to bridge over large regions of mostly closed field situated above the equator to join at the streamer belt cusp near a height of 2 $R_\odot$). The red line on each map shows the region where field lines of opposite polarity exist—this is the neutral line, or heliospheric current sheet, which is commonly used as a proxy for the coronal density structure. The topological correspondence between the convergence maps (right column) and the SRT density map (left column) is good, although the exact spatial configurations disagree. For CR 1912.5, the convergence map shows that the splitting of the streamer belt into two branches near longitude 270° is a consequence of large convergence along two separate branches. For CR 1917.5, the splitting of the streamer belt into three distinct branches near longitude 270° is clearly associated with a three-way branching of the convergence. For the same period, the splitting of the streamer belt into two narrow bands near longitude 45° is accompanied by a small but intense branching in the convergence map. The reasonable qualitative agreement between SRT density maps and PFSS convergence maps shows that the large-scale structure of the extended corona is dictated by the evolution of the coronal magnetic field from the photosphere to the extended corona: therefore the large-scale coronal field must be quasipotential.

As shown in Figure 2, the distribution of high-density sheets is constrained by the magnetic field configuration (or the convergence of the field). Where there is a bend in the heliospheric current sheet near longitude 270°, there is almost always a branching of the convergence sheets, and a corresponding branching of the density structure (with the exception of CR1919.5). Therefore, there is almost always higher density structure to be found near the high-convergence regions estimated by PFSS models. However, the actual distribution of density along the streamer belt can vary—seemingly without constraint by the shape of the belt. See, for example, how the regions of highest density (red regions) move in the density maps of Figure 2. These are not constrained to remain in the same place for long periods.

Integrating the densities shown in the left column of Figure 2 over latitude, and stacking them in time, gives the black line plots in Figure 3(a). The interesting structural insight given by the tomography is gone, but the integrated plots show the longitudinal movement of the largest-scale structure more clearly. This plot shows that the main highest density feature of the streamer belt drifts rather inconsistently in time, but with a general overall movement to lower longitudes between CR 1912.49 and 1918.49 with a mean rate of approximately −0.2 deg d^{-1} relative to the Carrington rate. After CR 1918.49, the rotation rate seems to reverse, with the main high-density feature returning to a longitude near 270°.

In a similar treatment as that applied to the density, the magnetic convergence shown in the right column of Figure 2 is integrated over latitude to give the red line plots of Figure 3(a). The interesting magnetic structure associated with the branches of high convergence near longitude 280° remains at roughly the same longitude—therefore it is rotating close to the Carrington rate. This movement is summarized in Figure 3(c). The bend

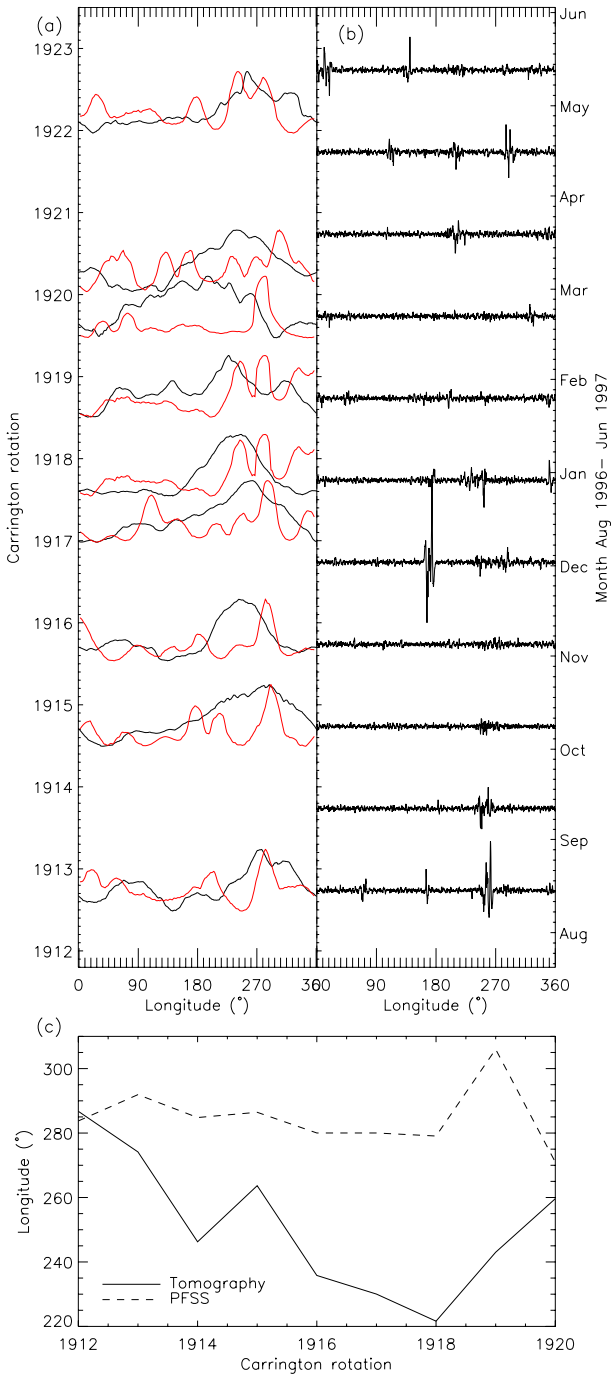

Figure 3. (a) Black lines: density integrated across all latitudes from each of the nine SRT density maps shown in the left column of Figure 2. For display purposes, each line plot is scaled from 0 to 0.75, then is plotted at the correct position on the *y*-axis. For example, the plot for the density map made for CR 1912.49 is placed at the bottom of the *y*-axis, with its minimum trough placed at CR 1912.49. Red lines: magnetic convergence integrated across all latitudes from the PFSS convergence maps of the right column of Figure 2. The integrated convergence is scaled and plotted in the same manner as the density. (b) Radial magnetic field integrated over latitude and plotted as a function of longitude from observations by MDI/*SOHO*. This value is plotted for several Carrington rotations, in a similar manner to (a). These plots serve to show the longitude of the main active regions on the disk. (c) The longitude of the maximum peak in SRT density (solid line) and PFSS convergence (dashed line), as a function of time during solar minimum. Since the density and convergence peaks are extended in longitude, their longitudinal positions are determined by fitting several Gaussians to the longitudinal profiles shown in (a). The longitude of the Gaussian with the highest peak is recorded at each time step. This procedure gives the approximate central position of the main high-density or high-convergence features—even when that feature consists of several closely distributed smaller peaks.

in the PFSS neutral sheet (dashed line) actually remains at an approximately constant longitude while the density structure (solid line) drifts to lower longitudes. That the density structure can drift independently of the more stable magnetic structure, before rapidly returning to a similar configuration, gives insight to the nature of the corona. The density structure is of course not separable from the magnetic structure, but there is a flexibility for density structures to move along the heliospheric current sheet, and such movement can be rapid.

Flux modulation measurements of the same period by Lewis et al. (1999) and Giordano & Mancuso (2008) have been used to calculate coronal rotation rates. They give rates of ~ -0.2 deg d^{-1} relative to the Carrington rate, with relatively low error bars. The tomography reveals that such a rotation rate is an average value which is correct only for a short six-month time period. Flux modulation studies depend on extended time series of observations ($\sim$1 yr) and do not attempt to decipher the coronal structure along the LOS. They do not reveal the interesting structural activity, and are based on the false assumption that the corona does not change density structure over long timescales. While this study shows that the magnetic structure may stay reasonably stable for a period of $\sim$six months during solar minimum, the density structure is shown to change more rapidly. Furthermore, the rotational characteristics of the magnetic corona, as determined by Hoeksema & Scherrer (1987) using a PFSS model, are not a reliable measure of the rotational characteristics of the electron density corona. Any flux modulation study of the solar minimum corona for latitudes more than a few degrees from the equator will be dominated by the persistent structure of the streamer belt splitting near 270°. The flux modulation measurement therefore is a confusion of the rotation of the magnetic structure and density features within that structure. This study shows that the density feature is not firmly anchored by the large-scale magnetic structure in the longitudinal direction.

An interesting question which arises from this study is what mechanism controls the distribution of density within the magnetic structure? A natural candidate for investigation would be magnetic activity on the disk. In Figure 3(b), the longitudinal distribution of active regions is shown for several consecutive Carrington rotations throughout the period of investigation. To create these profiles, the radial magnetic field calculated from LOS magnetograms by the Michelson Doppler Imager (MDI) instrument aboard *Solar and Heliospheric Observatory* (*SOHO*; Scherrer et al. 1995) are integrated over latitude. Active regions on the disk show up as strong neighboring peaks and trough pairs in these longitudinal profiles. There seems to be considerable magnetic activity associated with the interesting coronal structure near longitude 270° throughout the period, although the activity diminishes from CR 1917 to 1920, before reappearing strongly at CR 1921. A very strong active region appears at longitude $\sim$170° at CR 1916, but rapidly decreases in intensity by CR 1918. Other active regions appear and disappear, or move, quite rapidly. From comparing Figures 3(a) and (b), there seems to be little direct correspondence between rapid magnetic activity on the disk and magnetic or density activity in the corona. Rapid emergence and subsequent dissipation of large and intense active regions near the equator form spectacular arcades of loops which extend a considerable distance into the corona in extreme-ultraviolet images, but do not directly and instantly influence the streamer belt magnetic structure and density at larger heights. This is because the convergence sheets which form the streamer belt in the corona are open field line

structures arising from mid-latitudes (Morgan & Habbal 2010b), and are associated with the largest-scale and longest-lasting magnetic structures. The open fields which arise from mid-latitudes and converge near the equator, forming the streamer belt, bridge over magnetic structures which form at lower heights near the equator. Undoubtedly, the coronal magnetic field is affected, and is replenished, by the appearance and dissipation of active regions (Wang & Sheeley 2004; Fisk 2001; Lionello et al. 2005), but the global coronal response to active region emergence is complicated, not immediate, and not directly localized at the active region site. What effect the active regions have on coronal density distribution is less clear.

4. CONCLUSIONS

Density maps calculated using tomography from the observations of the LASCO C2 coronagraph are compared to magnetic convergence maps calculated from PFSS models. This comparison gives fresh insight into the evolution of coronal density structures during solar minimum (1996–1997). Our findings are as follows.

1. The topology of the equatorial streamer belt as revealed using SRT shows that PFSS models are often qualitatively correct. However, the PFSS models must be interpreted in terms of convergence and not solely by the magnetic neutral line.
2. The magnetic structure of the corona as revealed by PFSS must not be used as an accurate quantitative estimate of the true distribution of magnetic/density structure. The PFSS model results, while being topologically correct, can give inaccurate spatial estimates. Other observational constraints must be used alongside the PFSS results.
3. Structures of higher density in the main streamer belt can drift longitudinally. Their movement is constrained by the framework dictated by the magnetic field.
4. Density distribution changes more rapidly than magnetic structure.
5. The longitudinal drift of the main high-density structure between CR1912 and 1918 gives a mean rotation rate of -0.2 deg d^{-1} relative to the Carrington rate, while the magnetic structure drifts in the opposite direction (rotating slightly faster than the Carrington reference frame). PFSS models cannot therefore be used to predict the rotation of the electron corona, nor the exact distribution of density.
6. Flux modulation studies are not reliable indicators of coronal rotation since the true coronal movement is one of magnetic structural reconfiguration plus large-scale drifts of plasma within that structure. It is sometimes difficult to interpret rotation rates of a structure which is changing shape rapidly.

I am indebted to Shadia Habbal for invaluable advice and insight regarding this work. I am very grateful to an anonymous referee whose comments greatly improved the article. This work is supported by an NSF SHINE Award AGS-0962716, and NASA grants NNX07AH90G and NNX08AJ07G to the Institute for Astronomy. The *SOHO*/LASCO data used here are produced by a consortium of the Naval Research Laboratory (USA), Max-Planck-Institut fuer Aeronomie (Germany), Laboratoire d'Astronomie (France), and the University of Birmingham (UK). *SOHO* is a project of international cooperation between ESA and NASA. The Wilcox Solar Observatory's coronal field extrapolations were obtained from the WSO section of Stanford University's Web site courtesy of J. T. Hoeksema. WSO is supported by NASA, the NSF, and ONR.

REFERENCES

Altschuler, M. D., & Newkirk, G., Jr. 1969, Sol. Phys., 9, 131
Brueckner, G. E., Howard, R. A., Koomen, M. J., et al. 1995, Sol. Phys., 162, 357
Fisk, L. A. 2001, J. Geophys. Res., 106, 15849
Frazin, R. A. 2000, ApJ, 530, 1026
Giordano, S., & Mancuso, S. 2008, ApJ, 688, 656
Hoeksema, J. T., & Scherrer, P. H. 1987, ApJ, 318, 428
Kramar, M., Jones, S., Davila, J., Inhester, B., & Mierla, M. 2009, Sol. Phys., 259, 109
Lewis, D. J., Simnett, G. M., Brueckner, G. E., et al. 1999, Sol. Phys., 184, 297
Lionello, R., Riley, P., Linker, J. A., & Mikić, Z. 2005, ApJ, 625, 463
Morgan, H. 2011, ApJ, 738, 189
Morgan, H., & Habbal, S. 2010a, ApJ, 711, 631
Morgan, H., & Habbal, S. R. 2007, A&A, 464, 357
Morgan, H., & Habbal, S. R. 2010b, ApJ, 710, 1
Morgan, H., Habbal, S. R., & Lugaz, N. 2009, ApJ, 690, 1119
Morgan, H., Habbal, S. R., & Woo, R. 2006, Sol. Phys., 236, 263
Roša, D., Brajša, R., Vršnak, B., & Wöhl, H. 1995, Sol. Phys., 159, 393
Saez, F., Zhukov, A. N., Lamy, P., & Llebaria, A. 2005, A&A, 442, 351
Schatten, K. H., Wilcox, J. M., & Ness, N. F. 1969, Sol. Phys., 6, 442
Scherrer, P. H., Bogart, R. S., Bush, R. I., et al. 1995, Sol. Phys., 162, 129
Vásquez, A. M., Frazin, R. A., & Manchester, W. B. 2010, ApJ, 715, 1352
Wang, Y.-M., & Sheeley, N. R., Jr. 1992, ApJ, 392, 310
Wang, Y.-M., & Sheeley, N. R., Jr. 2004, ApJ, 612, 1196
Wang, Y.-M., Sheeley, N. R., Jr., & Rich, N. B. 2007, ApJ, 658, 1340